Journal of Nanobiotechnology

RESEARCH Open Access

A multifunctional composite scaffold responds to microenvironment and guides osteogenesis for the repair of infected bone defects

Jiajia Sun[1†], Haidi Zhu[1†], Huan Wang[1], Jiaying Li[1], Bin Li[1*], Ling Liu[1*] and Huilin Yang[1*]

Abstract

Treating bone defect concomitant with microbial infection poses a formidable clinical challenge. Addressing this dilemma necessitates the implementation of biomaterials exhibiting dual capabilities in anti-bacteria and bone regeneration. Of particular significance is the altered microenvironment observed in infected bones, characterized by acidity, inflammation, and an abundance of reactive oxygen species (ROS). These conditions, while challenging, present an opportunity for therapeutic intervention in the context of contaminated bone defects. In this study, we developed an oriented composite scaffold containing copper-coated manganese dioxide (MnO_2) nanoparticles loaded with parathyroid hormone (PMPC/Gelatin). The characteristics of these scaffolds were meticulously evaluated and confirmed the high sensitivity to H^+, responsive drug release and ROS elimination. In vitro antibacterial analysis underscored the remarkable ability of PMPC/Gelatin scaffolds to substantially suppressed bacterial proliferation and colony formation. Furthermore, this nontoxic material demonstrated efficacy in mitigating ROS levels, thereby fostering osteogenic differentiation of bone marrow mesenchymal stem cells and enhancing angiogenic ability. Subsequently, the infected models of bone defects in rat skulls were established to investigate the effects of composite scaffolds on anti-bacteria and bone formation in vivo. The PMPC/Gelatin treatment exhibited excellent antibacterial activity, coupled with enhanced vascularization and osteogenesis at the defect sites. These compelling findings affirm that the PMPC/Gelatin composite scaffold represents a promising avenue for anti-bacteria and bone regeneration.

[†]Jiajia Sun and Haidi Zhu contributed equally to this work.

*Correspondence:
Bin Li
binli@suda.edu.cn
Ling Liu
liulingly@suda.edu.cn
Huilin Yang
suzhouspine@163.com

Full list of author information is available at the end of the article

Graphical Abstract

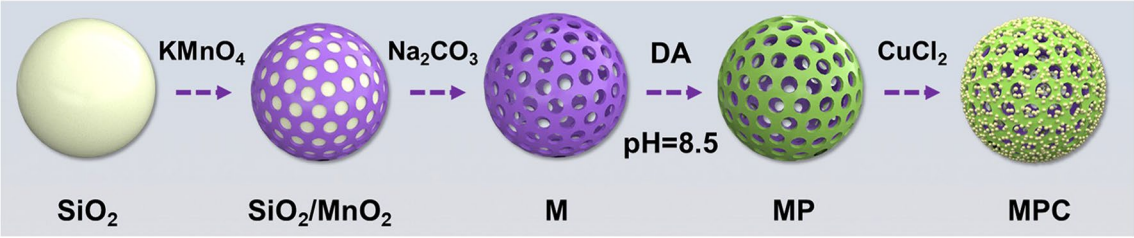

Keywords Anti-bacteria, Osteogenesis, Microenvironment response, Hollow manganese dioxide

Introduction

Implant materials have found extensive application in orthopedic fields to replace damaged tissue and restore functions. Despite the notable success achieved in this realm, challenges associated with implant failure remain a major concern [1]. In the United States, over one million total hip and knee replacements are conducted annually, with approximately one-third of these being revision surgeries [2]. Implant failure primarily stems from insufficient osteogenesis and implant-associated infection (IAI) [3, 4]. Of particular significance, IAI emerges as a critical postoperative complication [5]. Clinical data present that microbial contamination is the second leading cause for the failure of orthopedic implantation [6]. Meanwhile, effective bone regeneration in the infective defects is still a huge difficulty in clinical treatment [7]. Serious contamination of these sites may impede bone reconstitution, and lead to undesirable outcomes, such as tissue necrosis and septicemia [8, 9]. *Staphylococcus aureus (S. aureus)* stands out as the predominant pathogen responsible for chronic bone infections and osteomyelitis [10, 11]. Current approaches involve the administration of antibiotic injections intravenously and locally to combat bone bacterial infections. However, these methods are proven inadequate either due to the limited penetration of relatively low antibiotic concentrations at infected sites or the short duration of drug effectiveness [12, 13]. A promising avenue to address these challenges involves the development of dual-functionalized bone grafts, integrating anti-bacterial activity and osteo-induction. These innovative grafts are anticipated to fulfill the critical need for inducing effective bone formation in severely infectious defect sites.

Loading scaffolds developed for bone tissue engineering with various osteoinductive factors, such as growth factor, has been extensively investigated, yielding promising outcomes in enhancing osteogenesis. Recent researches have explored the incorporation of antibacterial agents, including antibiotics, to address infected bone defects. However, the utilization of non-antibiotic alternatives, such as ionic metals like copper (Cu) and silver, is imperative to mitigate antibiotic resistance. Cu, a well-established inorganic metal, exhibits excellent antimicrobial properties against both gram-positive and gram-negative bacteria as well as fungi [14]. Notably, nearly 300 Cu-based antibacterial products have registered with the United States Environmental Protection Agency, and these products are able to eradicate pathogenic bacteria up to 99.9% [15, 16]. Furthermore, Cu has been validated for its advantageous roles in osteogenic and angiogenic stimulation [17]. Cu ions could facilitate collagen maturation and osteogenic differentiation to increase bone mass [18, 19]. What's more, Cu's ability to stimulate bone mesenchymal stem cells (BMSCs) to secrete vascular endothelial growth factor (VEGF) contributes to its effect on vascular stimulation [17, 20]. Although antimicrobial materials have broad prospects in regenerative medicine, there is a trade-off between the ability to kill bacteria and the toxic effect on healthy cells in vivo. Consequently, the quantity of Cu employed becomes crucial. One viable strategy for regulating Cu dosage involves using a carrier to achieve localized delivery to the defect site and control its release kinetics.

To our understanding, the microenvironment within an infected bone milieu tends to be mildly acidic (pH 5.5–6.7), attributed, in all likelihood, to the production of lactic acid by microorganisms [21, 22]. Dramatically, infections induced by methicillin-resistant *S. aureus* (MRSA) can cause pH values to decrease to 5.5 or even lower [23]. Upon bone infection, the infiltration of polymorphonuclear leukocytes (PMN) into the infected site is a consequential response, with attempts made to engulf infective tissues. As a result, bone loss occurs by the release of high-active oxidants from activated PMN [24]. Prior investigations have documented osteomyelitis as a condition marked by a state of pronounced oxidative stress, significantly disrupting the delicate balance between osteoblastogenesis and osteoclastogenesis [25].

Therefore, the unique microenvironment associated with bone infection presents an opportunity to engineer responsive biomaterials capable of both bacterial eradication and fostering bone formation.

Nanoparticles (NPs) made from manganese dioxide (MnO_2) have garnered recent attention in medical science on account of their high sensitivity to H_2O_2 and H^+, which are abundant in tumors and osteoarthritis [26, 27]. Yang et al. introduced a hollow MnO_2 nanoplatform specifically tailored for the controllable release of therapeutic molecules in the tumor micro-environment characterized by slight acidity and H_2O_2 [28]. In a study of osteoarthritis, MnO_2 NPs have been noted to mitigate oxidative stress-induced cartilage inflammation [29]. Previously, our research team designed a MnO_2-embedded composite hydrogel with the capability to target endogenous H_2O_2 at the bone injury site, thereby promoting bone regeneration [30]. Nevertheless, the application of MnO_2 NPs on designing an intelligent antibacterial system within the microenvironment of bone infection remains insufficiently explored.

Metal ions are typically deposited or sprayed onto implant surfaces using various methods such as micro-arc oxidation and plasma spray techniques [31]. However, inspired by the mechanism of mussel adhesion, polydopamine (PDA) has introduced new possibilities for the surface functionalization and biomedical applications of nanoparticles as drug carriers. This is due to its unique properties, including exceptional adhesiveness, excellent biocompatibility, and mild synthesis requirements [32]. PDA can form and adhere to almost all material surfaces, including metals, ceramics, semiconductors, and synthetic polymers [33]. Additionally, its catechol structure provides strong coordination with polyvalent metal ions, such as iron, zinc, and copper ions [34]. Consequently, PDA can indirectly adsorb other molecules through metal ion coordination. We hypothesize that the unique properties of PDA can facilitate the coating of copper onto the surface of MnO_2 NPs.

Beyond its anti-infective properties, fostering favorable osteo-induction is imperative for repairing infectious bone defects. Parathyroid hormone (PTH) serves as a key endocrine regulator, influencing extracellular calcium and phosphate levels and exerting a pivotal impact on bone metabolism [35]. Notably, PTH is the sole osteoporosis drug approved by the Food and Drug Administration (FDA) for promoting neo-bone regeneration [36]. Numerous studies on animal models have consistently illustrated the efficacy of PTH injections in enhancing bone boss and fracture healing [37, 38]. In a human case study, persistent non-union following attempts at autograft, external fixation, and internal fixation with bone morphogenetic protein-7 (BMP-7) was resolved only upon the off-label use of PTH [39]. Hence, PTH emerges as a potent stimulator of bone formation, presenting itself as a viable substitute for autograft and BMP in the treatment of bone defects. Exploring the application of a biomaterial system for localized PTH release at defect sites holds promise as a method to method to facilitate bone regeneration and healing.

In this study, we aimed to develop PTH-loaded Cu-coated hollow MnO_2 (PMCP) NPs with the responsivity to increased acidity and the ability to scavenge reactive oxygen species (ROS). Subsequently, PMCP NPs were dispersed into gelatin solution to fabricate oriented composite scaffolds using the freeze casting technique. Under conditions of excessive H_2O_2 or acidic pH inherent in cells and tissues, the NPs underwent degradation, facilitating the release of PTH and Cu ions. The simultaneous release of PTH and Cu ions not only exhibited antibacterial efficacy, but also improved cell growth and osteogenic differentiation by eliminating ROS, thus accelerating the healing process in infected bone. Form these findings, we anticipate that the multifunctional scaffold could achieve high antibacterial efficiency and promote bone healing against the adverse infection microenvironment (See Scheme 1).

Methods and materials

Synthesis and characterization of hollow Cu-coated MnO2 NPs

Hollow MnO_2 NPs were synthesized as previously reported. Briefly, 2 mL of deionized water (DIW, 2 mL), ethanol (14 mL), and $NH_3{\cdot}H_2O$ (500 μL) were mixed at 50 °C for 5 min in an oil bath under stirring. And then, tetraethyl orthosilicate (500 μL) was dropwise added into the mixture, stirred at 50 °C for 2 h, and finally SiO_2 NPs were obtained. For SiO_2@MnO_2 NPs synthesis, 3% $KMnO_4$ solution (20 mL) was dropwise added into the SiO_2 NPs under ultrasound and obtained mixture was continued by ultrasound for 1 h and then stirred at room temperature (RT) for 12 h to gain SiO_2@MnO_2 NPs. Finally, the resulting SiO_2@MnO_2 NPs were dissolved in Na_2CO_3 solution at 60 °C for 24 h in an oil bath. The obtained hollow MnO_2 NPs were washed with DIW five times.

For the synthesis of hollow Cu-coated MnO_2 NPs, the polydopamine (PDA) was first coated on the surface of hollow MnO_2 NPs (MP). MnO_2 NPs (120 mg) were evenly dispersed into DIW (15 mL) in a flask under ultrasound. Then dopamine (12 mg, Sinopharm Chemical Reagent Co., Ltd, Shanghai, China) was dissolved in DIW (5 mL) and then added into the above flask. $NH_3{\cdot}H_2O$ (200 μL) was added into the mixture, which was stirred at 45 °C for 4 h in an oil bath. The collected products were dispersed into $CuCl_2$ solution (10 mL) and stirred overnight at RT. The hollow Cu-coated MnO_2 (MPC) NPs were centrifugation and washed with DIW and ethanol

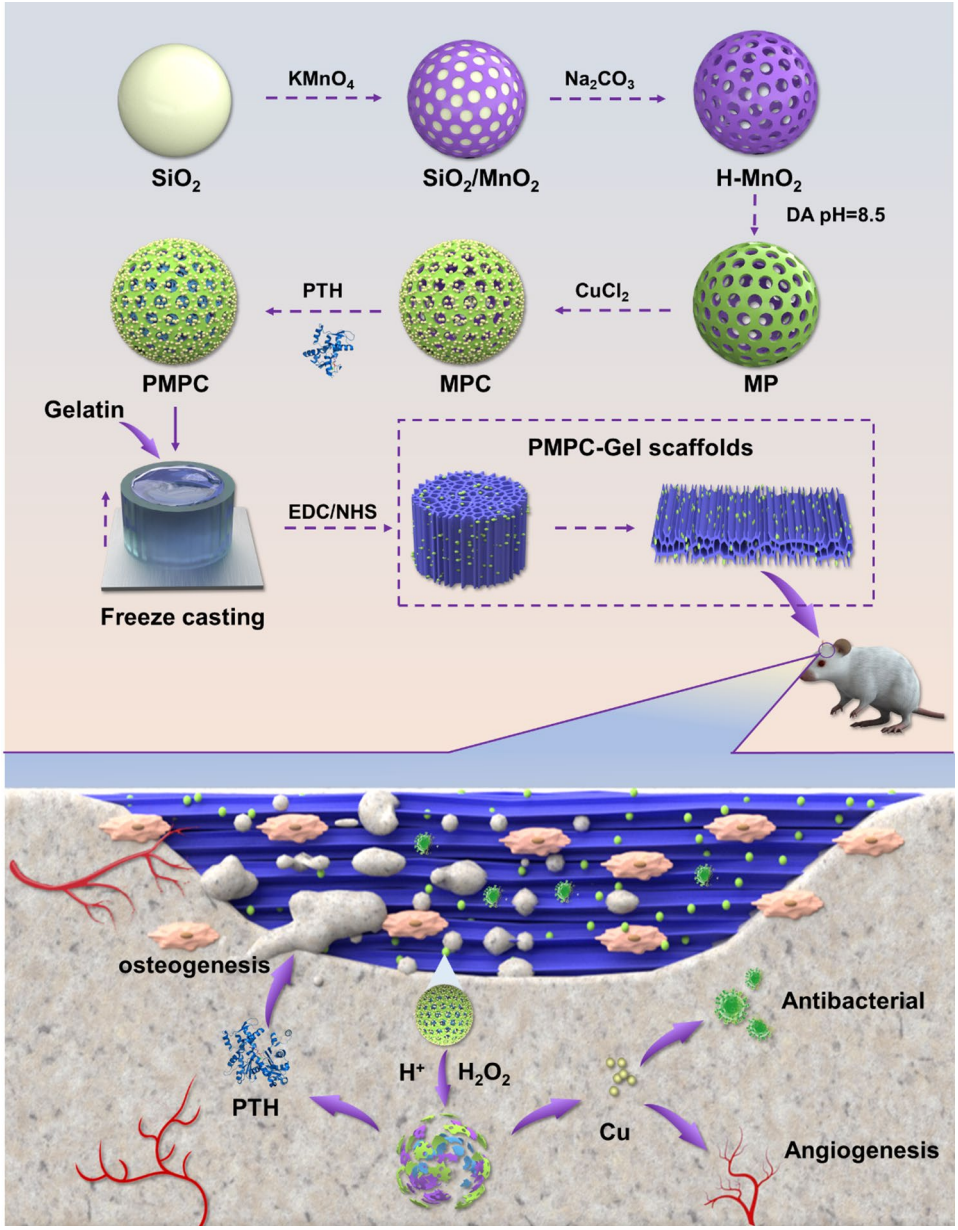

Scheme 1 Schematic illustration of the preparation of an oriented gelatin scaffold containing Cu-coated MnO_2 NPs loading PTH for the repair of contaminated bone defects. MnO_2 NPs are able to respond to ROS in the infected microenvironment, scavenging ROS and generating oxygen, and accordingly resulting in the release of PTH and Cu. These released substances could exert the effects on antibacterial, vascularization and bone formation. Abbreviation, H-MnO_2: hollow manganese dioxide, DA: dopamine, MP: polydopamine-coated MnO_2, MPC: Cu-coated MP, PTH: parathyroid hormone, PMPC: PTH-loaded MPC, EDC: 1-ethyl-3-(3-dimethylaminopropyl) carbodiimide, NHS: N-hydroxy succinimide

several times. Energy-dispersive X-ray spectroscopy detector system (EDS, Oxford X-MAX, Oxford, UK) and transmission electron microscopy (TEM, FEI Tecnai F20, Hillsboro, OR, USA) were used for elemental analysis and surface morphology observation of NPs, respectively.

Cytotoxicity assay in vitro

The MnO_2NP cytotoxicity was determined by examining the viabilities of rat BMSCs (rBMSCs) treated with NPs utilizing CCK-8 assay (Solarbio, Beijing, China). Briefly, rBMSCs (1×10^3 per well) were plated on a 96-well plate and allowed to adhere overnight. Subsequently, 24 h of incubation with NPs, the cell culture medium was aspirated, and 90 μL fresh culture medium was evenly mixed with 10 μL CCK-8 reagent, which was added for an additional 2-hour incubation to induce color formation. The absorbance was measured at 450 nm wavelength. Besides, the cytotoxicity of MnO_2 NPs coated with different concentrations of Cu^{2+} was also tested using the CCK-8 assay at 3 and 5 days.

Preparation of oriented composite gelatin scaffolds

3 g Gelatin was evenly dissolved 60 mL DIW at 60 ℃, and then 0.3 g NPs were added into the gelatin solution and stirred at a speed of 200 rpm for 30 min to form a homogeneous solution. As described previously, the mixture was poured into a homemade model using a freeze-casting technique. The obtained oriented scaffolds were directly cross-linked by a mixed solution of EDC (50 mM) and NHS (25 mM). The morphological and microstructural study of the synthesized scaffolds was observed using scanning electron microscopy (SEM: Quanta 250, FEI, Hillsboro, OR, USA).

Cytoskeleton staining

rBMSCs were cultured on the surface of composite scaffolds at a density of 1×10^4 per well to observe cell morphology on composite scaffolds. After 24 h of culture, the cells underwent fixation in 4% paraformaldehyde (PFA) for 30 min, followed by permeabilization with 0.5% Triton X-100 for 15 min. Subsequently, TRITC-phalloidin solution (MCE, NJ, USA) was employed for cell staining, and the nuclei were counterstained using DAPI solution (Beyotime, Shanghai, China). Visualization was achieved using a fluorescence microscope (Zeiss Axiovert 200, Carl Zeiss Inc, Thornwood, NY, USA).

Drug release

Bovine serum albumin (BSA) released from the MPC NPs and MPC/Gelatin composite scaffolds was quantified in vitro by a BCA protein assay kit (Solarbio, Beijing, China) to investigate the stimuli-responsive property of NPs at different pH values (6.4 and 7.2). The solution was collected at predetermined intervals, and equal amounts of fresh PBS were added to continue the release process. All collected solutions were stored at -20 °C for subsequent analysis.

Live/Dead staining

Cultivation of rBMSCs at a density of 1×10^4 cells per well took place in the lower compartment of a 24-well transwell plate. Subsequent to cellular attachment, a treatment with 100 μM H_2O_2 was administered, and the upper chamber received the introduction of composite scaffolds. The control group (CTRL) was established with an empty upper chamber. Evaluation using a live/dead staining kit was performed after a 24-hour culture.

Cell proliferation

rBMSCs were cultured in the lower chamber of a 24-well transwell plate at a density of 1×10^3 cells per well. After 12 h, the composite scaffolds were placed in the upper chamber. The blank upper chamber was defined as the control group (CTRL). Cell proliferation was examined using the CCK-8 assay at 1, 3, and 5 days.

Senescence-associated β-galactosidase (SA-β-Gal) staining

rBMSCs (1×10^3 cells per well) were cultured in the lower chamber of a 24-well transwell plate. After attachment, cells were treated with 100 μM H_2O_2 and the composite scaffolds were placed in the upper chamber. After co-cultured for 3 days, cells were fixed and stained with a β-galactosidase solution (Beyotime, Shanghai, China) overnight at 37 °C. The cells were observed by a light microscope.

Intracellular ROS assay

rBMSCs co-cultured with composite scaffolds in the presence of 100 μM H_2O_2 for 24 h was followed by exposure to a DCFH-DA solution (10 μM, Beyotime, Shanghai, China) at 37 °C for another 1 h. Visualization was achieved using a fluorescence microscope.

Mitochondrial membrane potential assay

The Mito-Tracker red staining was performed to detect mitochondrial activity. After 24 h of rBMSCs and composite scaffolds co-culture in the presence of 100 μM H_2O_2, Mito-Tracker Red CMXRos working solution (200 nM, Beyotime, Shanghai, China) was added into each well of 24-well transwell plate and the samples were incubated at 37 °C for 30 min. Then, the working solution was removed and the rBMSCs were visualized using a fluorescence microscope.

ALP and alizarin red staining

After treated with 100 μM H_2O_2 for 3 days, rBMSCs were co-cultured with composite scaffolds in the absence of H_2O_2. After another 7-day culture, the cells were fixed and incubated with an ALP staining solution (Beyotime, Shanghai, China). After another 14-day culture, the cells were fixed and stained with an alizarin red solution (Beyotime, Shanghai, China). Then, quantitative analysis of alizarin red staining was detected using a perchloric acid solution.

Real-time quantitative polymerase chain reaction (RT-qPCR) analysis

Total RNA was extracted from rBMSCs using a TRIzol reagent (Invitrogen, Carlsbad, CA, USA). After RNA concentration measured, 1 μg of RNA was reverse-transcribed into cDNA and thereby RT-qPCR was performed to compare the gene changes of different treatments. The primer sequences of the genes (Sangon Biotech, Shanghai, China) are listed in Table 1. In order to analyze the relative changes in mRNA level, each gene expression was normalized by *Gapdh* and calculated using the $2^{-\Delta\Delta CT}$ method.

Table 1 Primers for RT-qPCR

Gene	Forward (5′-3′)	Reverse (5′-3′)
AlpL	TATGTCTGGAACCGCACTGAAC	CACTAGCAAGAAGAAGCCTTT
Runx2	ATCCAGCCACCTTCACTTACACC	GGGACCATTGGGAACTGATAG
Spp1	GCGGTTCACTTTGAGGACAC	TATGAGGCGGGGATAGTCTTT
Bglap	AACGGTGGTGCCATAGATGC	AGGACCCTCTCTCTGCTCAC
Col1a1	CAGGCTGGTGTGATGGGATT	CCAAGGTCTCCAGGAACACC
Sirt1	ACGCCTTATCCTCTAGTTCCTGTGG	CGGTCTGTCAGCATCATCTTCCAAG
Sod1	CGGCTTCTGTCGTCTCCTTGC	AACTGGTTCACCGCTTGCCTTC
Cat	GGCCTGACTGACGCGATTGC	CTGCTCCTTCCACTGCTTCATCTG
Gapdh	GACATGCCGCCTGGAGAAAC	AGCCCAGGATGCCCTTTAGT

Immunofluorescence

rBMSCs were fixed with 4% PFA and permeabilized by 0.1% Triton X-100 in PBS. After blocking, cells were incubated overnight at 4 °C with primary antibodies including Col-I (1:400, ABclonal, Boston, MA, USA). Subsequently, the samples were stained with the respective secondary antibodies labeled by cy3 (Beyotime, Shanghai, China) and FITC-Phalloidin (Yeasen, Shanghai, China) for 1 h at RT. The nuclei were counterstained with DAPI and then images were acquired using a fluorescence microscope.

Vascularization-related assays in vitro

For wound healing assays, HUVECs were plated in the lower compartment of 6-well transwell plates at a density of 5×10^5 cells per well and incubated until reaching 100% confluence. A sterilized 1 mL pipet tip was used to create a "scar" without cells in the middle of each well. After washed, fresh culture mediums with 1% FBS and 100 μM H_2O_2 were added to the corresponding well, and then composite scaffolds was put in the upper chamber. Crystal violet staining was performed at 24 h of co-culture.

For the transwell migration assay, 24-well transwell plates with 8 μm pore size were utilized, wherein composite scaffolds were positioned in the lower chamber. On the upper chamber, HUVECs were seeded. Following a 6-hour co-culture period in the presence of 100 μM H_2O_2, cells underwent fixation and staining with a crystal violet solution. The number of migrated cells was quantified using ImageJ software.

For the tube formation assay, HUVECs were plated in the lower chamber of 24-well transwell plates coated with Matrigel (BD Biosciences, USA), while composite scaffolds were placed in the upper chamber. Following a 24-hour co-culture period in the presence of 100 μM H_2O_2, cells were stained with Calcein-AM for 20 min at 37 ℃. Subsequently, images were captured using a fluorescence microscope, and the total branch points and total tube length were evaluated using ImageJ software.

Antibacterial tests in vitro

S. aureus and *Escherichia coli (E. coli)* were used to evaluate the antibacterial characteristics of the composite scaffolds. *S. aureus* (1×10^6 CFU/mL) and *E. coli* (1×10^6 CFU/mL) were co-incubated with different scaffolds in a 24-well plate and incubated for 24 h at 37 °C, respectively. Samples were washed with PBS several times to remove non-attached bacteria. Subsequently, 1 mL PBS was added into each well, and the attached bacteria were detached into PBS under ultrasound. After 10 times dilution, bacterial suspension (20 μL) was spread on agar plates and then cultured at 37 °C for 12 h. Afterward, the number of active CFUs was counted and imaged.

Establishment of infected bone defects

We followed the NIH Guide for the Care and Use of Laboratory Animals and obtained approval from the Institutional Animal Care and Use Committee of Soochow University (SUDA20220711A09). Sixty Sprague-Dawley rats, aged 8 to 10 weeks, were randomly assigned to one of the following five groups: Defect, M/Gelatin, MP/Gelatin, MPC/Gelatin and PMPC/Gelatin. The animals were scheduled for harvesting at 1, 4, and 8 weeks post-surgery. Different composite scaffolds were contaminated with *S. aureus* bacterial suspension (1×10^6 CFUs/mL), which were placed at 37 °C for 6 h under a wet condition to allow bacterial attachment. Subsequently, a full thickness skull defect of 5 mm in diameter was created with a trephine, and treated scaffolds were gently implanted into the defect sites.

Anti-infection evaluation in vivo

The scaffolds were taken out from one defect in each group for microbiological examination one week after surgery. Then, the samples were homogenized for 5 min in 1 mL PBS. After filtration and 10 times dilution, bacterial suspension (20 μL) was spread onto an agar plate and cultured at 37 °C for 12 h. The viable bacterial counts were taken. Meanwhile, the scaffolds were obtained from another defect in each group for protein extraction. The level of IL-8 and TNF-α were tested by ELISA kits.

Micro-CT analysis

Samples harvested at four and eight weeks were scanned by micro-CT scanning (65 kV, 385 mA, 1 mm Al filter).

3D reconstruction images and quantitative analysis of BV/TV values were calculated.

Histological preparation

Four and eight weeks post-surgery, the samples were harvested, fixed and then decalcified one month. Following that, the cranial tissues were embedded in paraffin blocks, cut into 5 μm-thick sections, and stained with H&E stain, CD31, and OCN antibodies (Abcam, Cambridge, UK) to assess bone formation.

Statistical analysis

All experiments were repeated at least 3 times. All values are expressed as mean ± standard deviations. A one-way analysis of variance (GraphPad Software, San Diego, CA, USA) was performed along with Tukey's multiple comparison test to measure statistical differences between groups. P values < 0.05 were considered statistically significant.

Results

Synthesis and characterization of MPC NPs

Figure 1A illustrated the procedure for Cu-coated MnO_2 NP. We synthesized the hollow mesoporous MnO_2 (M) with silica as a template. Then, we treated the obtained NPs with dopamine solution to deposit a polydopamine (PDA) coating on the NP's surface to obtain MnO_2/PDA (MP) NPs. Finally, the Cu layer was accurately grown on the surface of the MP NPs by PDA reducibility to obtain Cu-coated MnO_2 (MPC) NPs. The TEM images of the M, MP, and MPC NPs exhibited the products' spherical morphology and hollow structure, confirming the hollow structure of NPs without residual SiO_2 (Fig. 1B). The corresponding EDS spectrum proved the presence of the Mn, O, C, N, and Cu elements derived from MPC NPs (Fig. 1C). These elemental mapping results further demonstrated that the MPC MPs contained Mn, O, C, and Cu (Fig. 1D).

Next, the CCK-8 assay revealed that the MnO_2 NPs did not exhibit toxicity to rBMSCs, even at high concentrations of up to 50 μg/mL (Fig. 1E). Hence, the MnO_2 NPs were used at a concentration of 50 μg/mL in further experiments. Additionally, the MP NPs were added into 0.02 M, 0.1 M, and 0.5 M $CuCl_2$ solution to obtain MPC-0.02, MPC-0.1, and MPC-0.5 NPs, respectively. CCK-8 assay results showed that rBMSCs treated with MPC-0.1 NPs had the highest cell activity among all groups at 3 and 5 days (Fig. 1F).

Characterizations of oriented composite scaffolds

The oriented composite scaffolds with different NPs were fabricated using unidirectional freeze-drying. The SEM micrographs of composite scaffolds demonstrated that the porous and oriented structure of the scaffolds could be observed, and the NPs were uniformly distributed in the scaffolds (Fig. 2A). Additionally, cells were stained with TRITC-conjugated phalloidin, a fluorescent probe that binds specifically to F-actin. rBMSCs cultured on the composite scaffolds exhibited an elongated cell shape and aligned parallel to the fiber direction (Fig. 2B).

Afterward, we investigated in vitro drug release of MPC NPs and MPC/Gelatin composite scaffolds to evaluate the loading and degradation characteristics. To better replicate the infected microenvironment, drug release behavior tests were conducted in both acidic (pH = 6.4) and neutral (pH = 7.2) PBS solution (Fig. 2C). The cumulative release curve demonstrated the sustained delivery of BSA for a minimum of 14 days. Notably, the release rate of BSA from MPC NPs was elevated in the acidic medium compared to the neutral medium. Approximately 80% of BSA was released from MPC NPs in the acidic medium within the 14-day timeframe, whereas it was less than 50% in the neutral medium. Moreover, incorporation of MCP NPs into the gelatin scaffolds resulted in a reduction in the BSA release rate, suggesting that the composite scaffold delivery system could enhance bioavailability, prevent abrupt drug release, and mitigate toxicity and side effects.

Protection of rBMSCs from oxidative damage by composite scaffolds

To evaluate the antioxidant defense capacity of MPC/gelatin composite scaffold, the rBMSCs were exposed to H_2O_2. Live/dead staining and CCK-8 assay discovered that H_2O_2 treatment increased the numbers of dead cells (red) and declined cell viability. However, treatment with M/gelatin, MP/gelatin and MPC/gelatin could suppress H_2O_2-induced effects, while gelatin treatment had no effect on H_2O_2 damage (Fig. 3A-C). Additionally, SA-β-Gal staining indicated that adding H_2O_2 to the culture medium for 3 days could induce cell senescence in rBMSCs. However, the cells in the M/Gelatin, MP/Gelatin and MPC/Gelatin groups all exhibited lower SA-β-Gal activity than cells in CTRL and Gelatin groups (Fig. 3D).

Antioxidant properties of composite scaffolds

The DCF fluorescence intensity was detected to investigate the ROS scavenging activity of MPC/Gelatin scaffolds using an ROS assay kit. The ROS content increased after H_2O_2 treatment, but decreased after treatment with M/Gelatin, MP/Gelatin and MPC/Gelatin. However, Gelatin treatment did not significantly reverse H_2O_2-induced ROS production (Fig. 4A). Mitochondria are major consumers of oxygen and potential ROS sources. ROS overproduction could lead to mitochondrial dysfunction, which in turn deteriorated oxidative stress. Mito-tracker Red CMXRos assays were conducted to investigate mitochondrial function. As a result, mitochondrial membrane

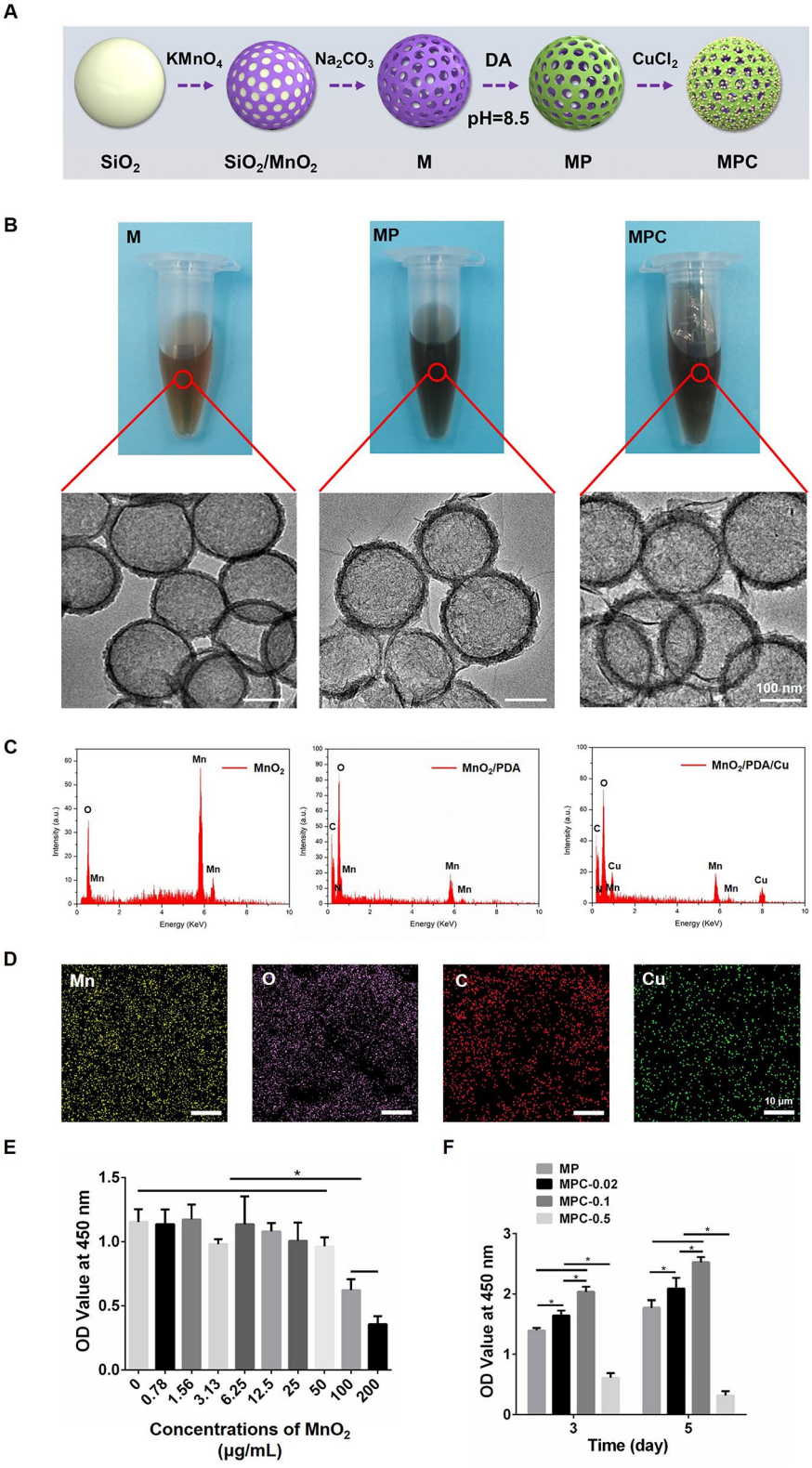

Fig. 1 Synthesis and characterization of MPC NPs. **(A)** A schematic representation indicating the synthesis process of MPC NPs. **(B)** Digital picture and TEM images of MnO_2, MP and MPC NPs. **(C)** EDS analysis of MnO_2, MP and MPC NPs. **(D)** EDS mapping of MPC NPs. **(E)** Relative viabilities of rBMSCs treated with various concentrations of MnO_2 NPs for 24 h. **(F)** Relative viabilities of rBMSCs treated with MPC NPs coated different Cu^{2+} concentrations at 3 and 5 days. *, $p < 0.05$

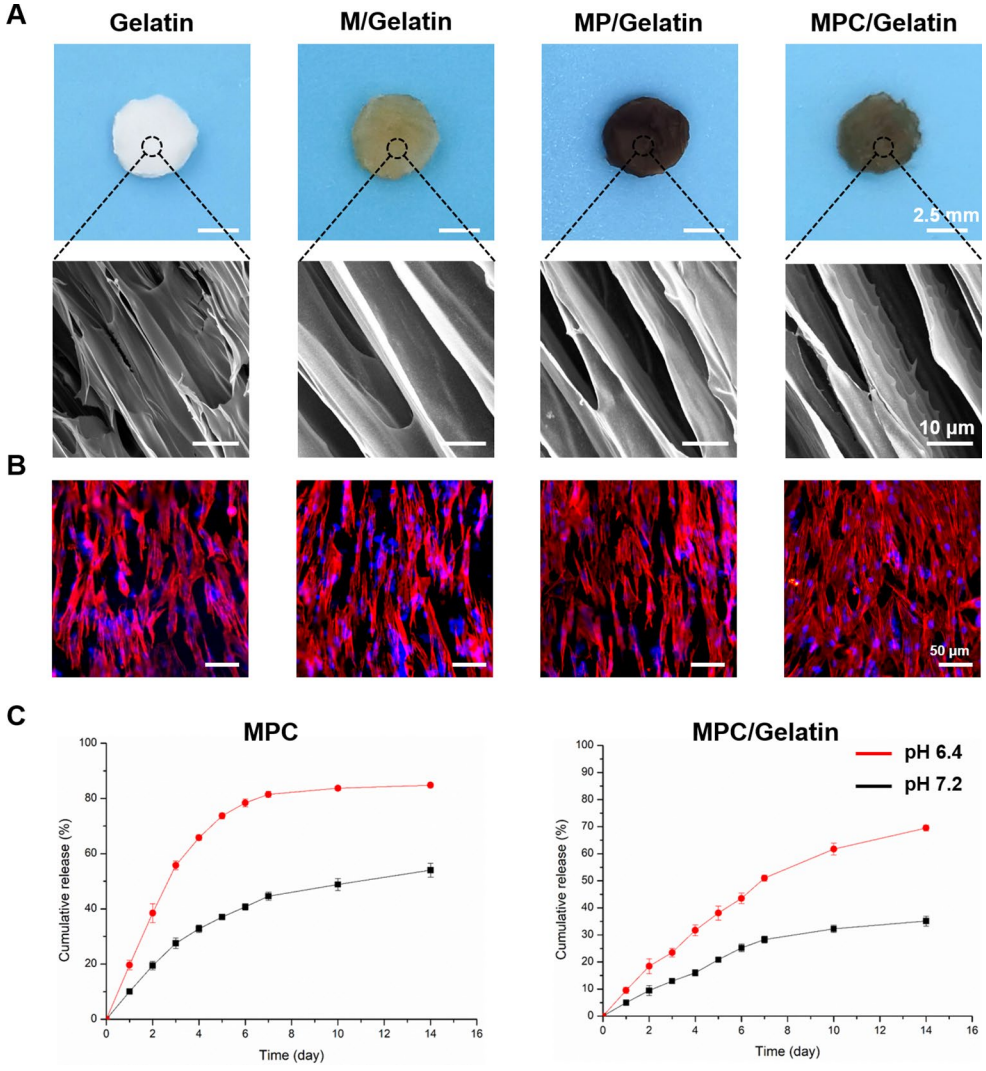

Fig. 2 Synthesis and characterization of MPC/Gelatin composite scaffold. **(A)** Digital picture and SEM images of Gelatin, M/Gelatin, MP/Gelatin and MPC/Gelatin composite scaffolds. **(B)** Cytoskeletal staining of rBMSCs seeded on the surface of Gelatin, M/Gelatin, MP/Gelatin and MPC/Gelatin composite scaffolds. Red and blue colors represent F-actin, and DAPI fluorescence, respectively. **(C)** Drug release properties of MPC NPs and MPC/Gelatin composite scaffold under acidic and neutral conditions

potential was higher in the cells treated with M/Gelatin, MP/Gelatin and MPC/Gelatin than in the cells of CRTL and Gelatin groups (Fig. 4B). In addition, antioxidative gene expressions, such as *Sirt1*, *Sod1*, and *Cat*, were significantly increased in cells treated with M/Gelatin, MP/Gelatin and MPC/Gelatin compared to cells treated with Gelatin under oxidative stress condition (Fig. 4C-E).

In vitro osteogenesis of cells cultured with composite scaffolds

Based on the above results, we found that gelatin scaffolds alone had weak or no biological effects on the response of rBMSCs to oxidative damage, while NP-loaded composite scaffolds could decrease ROS level and improve cell viability. PTH was encapsulated within MPC NPs to enhance bone formation more effectively and to investigate the osteogenesis of rBMSCs cultured with composite scaffolds in vitro. The cells were pre-treated with 100 μM H_2O_2 for 3 days, and osteogenic induction was performed for another 7 days. ALP staining and alizarin red staining were employed to determine ALP production and calcium deposition. ALP production increased dramatically, with the greatest increase in the PMPC/Gelatin group in the MPC/Gelatin and PTH-loaded MPC/Gelatin (PMPC/Gelatin) groups (Fig. 5A). Alizarin red staining analysis revealed a similar trend (Fig. 5B and C). Moreover, we performed RT-qPCR analysis to detect osteogenic gene expressions, including such as runt-related transcription factor 2 (*Runx2*), alkaline phosphatase (*Alpl*), secreted phosphoprotein 1 (*Spp1*), bone gamma-carboxyglutamate protein (*Bglap*), and collagen type I alpha 1 chain (*Col1a1*). The PMPC/Gelatin

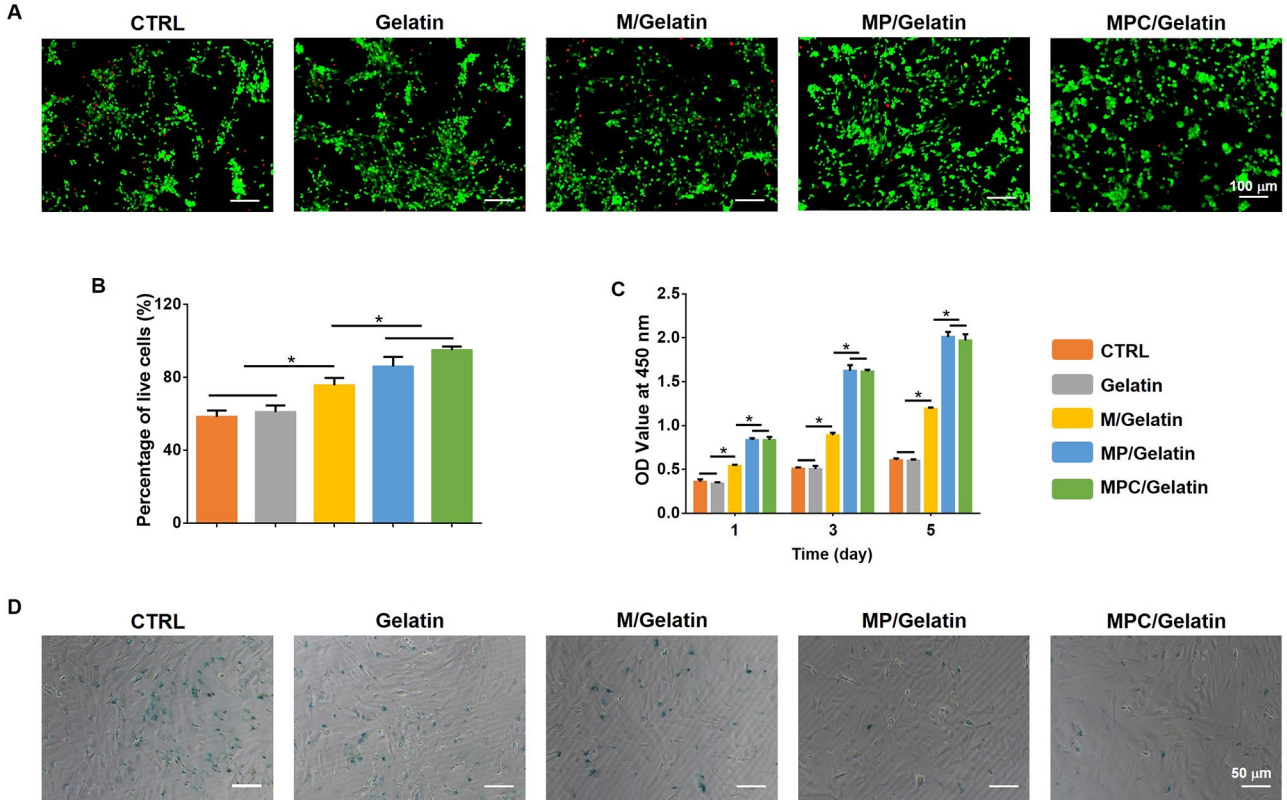

Fig. 3 Protective effects of MPC/Gelatin on rBMSCs. **(A)** Representative images of live/dead staining of rBMSCs treated with composite scaffolds in the present of 100 μM H_2O_2. **(B)** Quantification of the percentage of living cells in CTRL, Gelatin, M/Gelatin, MP/Gelatin and MPC/Gelatin groups, respectively. **(C)** CCK-8 assay of rBMSCs treated with composite scaffolds in the present of 100 μM H_2O_2. **(D)** Representative images of SA-β-Gal staining of rBMSCs treated with composite scaffolds in the present of 100 μM H_2O_2. *, $p < 0.05$

group significantly promoted osteogenesis-related gene expressions (Fig. 6A-E). Consistent with the RT-qPCR results, immunofluorescent analyses further showed that osteogenic-related protein, Col-I, was higher in the PMPC/Gelatin group compared with the other groups (Fig. 6F and G). Therefore, the results imply that persistent release of Cu^{2+} and PTH from the PMPC/Gelatin composite scaffolds synergistically facilitate the osteogenic differentiation of rBMSCs in vitro.

In vitro angiogenesis of HUVECs induced by composite scaffolds

Angiogenesis plays an essential role in the entire process of bone formation. Thus, to investigate the angiogenic effects of composite scaffolds on vascular endothelial cells, three classic experiments, including wound healing, transwell migration and tube formation, were carried out. The results of the wound healing and migration assays showed that HUVEC migration ability co-cultured with PMPC/Gelatin composite scaffolds was dramatically induced among all treatment groups (Fig. 7A-C). Further, tube formation assay found that a higher number of honeycomb-like structures were observed in the PMPC/Gelatin group, with increased total tube length and branch points, compared with other groups (Fig. 7D-F).

Anti-infection efficacy of composite scaffolds in vitro and in vivo

Figure 8A presented the antibacterial activity of composite scaffolds in vitro. We discovered that the MPC/Gelatin could completely inhibit the proliferation of *S. aureus* and *E. coli*, represented by few bacterial communities, compared to the other four groups (Fig. 8C). This result indicated that Cu^{2+} released from MPC/Gelatin led to the reduction of bacteria, and other materials used to synthesize composite scaffolds did not inhibit bacterial growth. Furthermore, we studied antimicrobial activity in vivo tests. We observed numerous bacterial colonies 7 days after the biomaterial implantation in Defect, M/Gelatin, and MP/Gelatin groups. The MPC/Gelatin and PMPC/Gelatin significantly reduced bacterial survival and colony numbers (Fig. 8B and D). This suggests that the Cu-coated NPs have strong antibacterial activity, consistent with our in vitro study. ELISA experiments demonstrated that tumor necrosis factor-α (TNF-α) and interleukin-6 (IL-6) expressions, common indicators of ongoing infections, decrease significantly in the MPC/

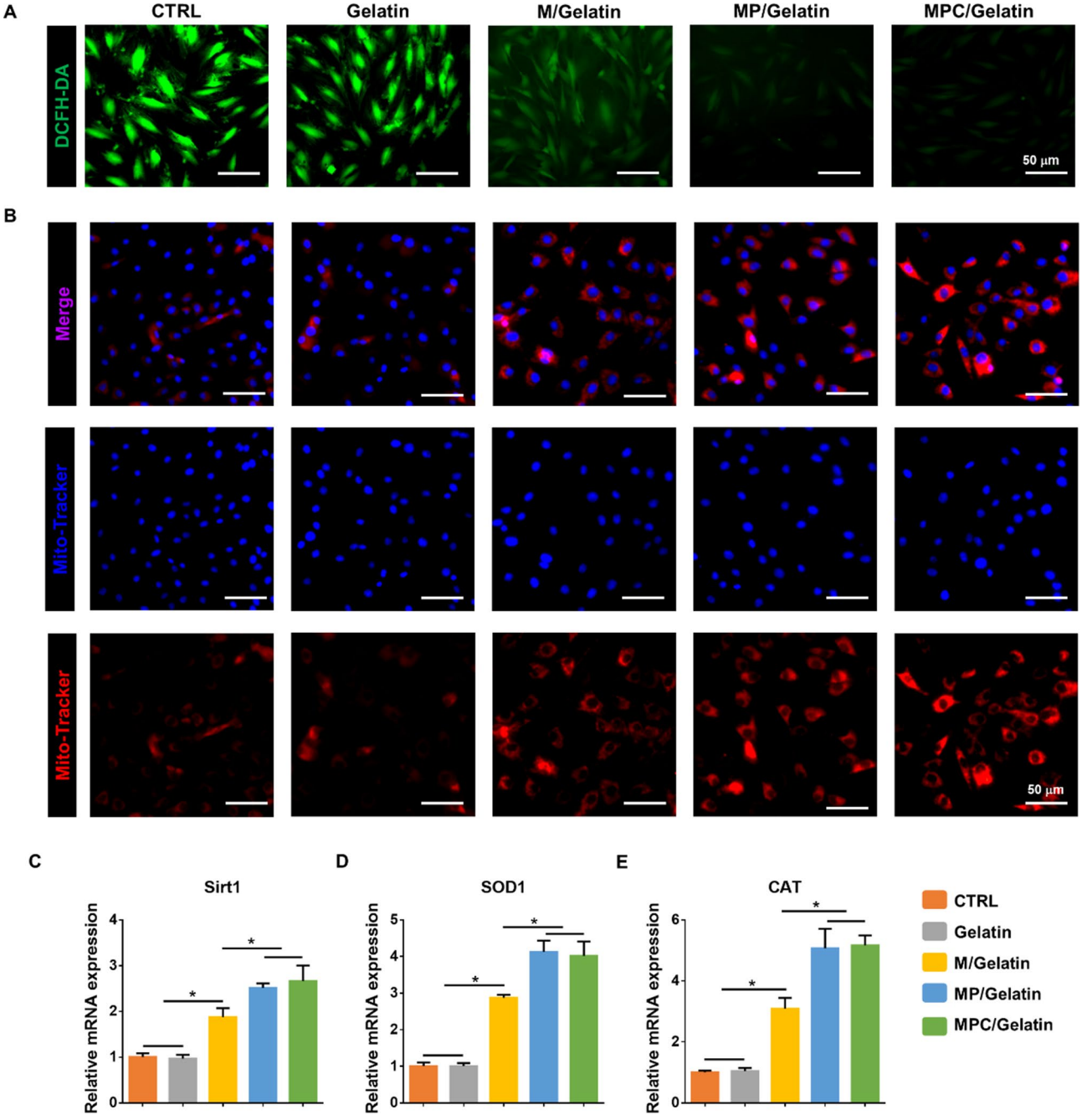

Fig. 4 Antioxidant properties of MPC/Gelatin composite scaffold. Representative fluorescent images of rBMSCs stained with DCFH-DA **(A)** and Mito-tracker **(B)** in CTRL, Gelatin, M/Gelatin, MP/Gelatin and MPC/Gelatin groups, respectively, in the present of 100 μM H_2O_2. **(C-E)** RT-qPCR analyses of relative expression of *Sirt1*, *Sod1*, and *Cat* genes of rBMSCs in CTRL, Gelatin, M/Gelatin, MP/Gelatin and MPC/Gelatin groups, respectively, in the present of 100 μM H_2O_2. *, $p < 0.05$

Gelatin and PMPC/Gelatin groups 7 days after implantation (Fig. 8E).

In vivo bone formation ability of composite scaffolds

We transplanted composite scaffolds into rat skull defects to evaluate their effects on infected bone repair. This study analyzed the bone volume fraction defect of the calvarial specimens using micro-CT at 4 and 8 weeks post-implantation. The results indicated that the new bone coverage area in all experimental groups was increased compared to the Defect group at 4 and 8 weeks, with the PMPC/Gelatin group having the highest bone content (Fig. 9A and B). Figure 9C presented H&E results. The newborn bone developed from the periphery

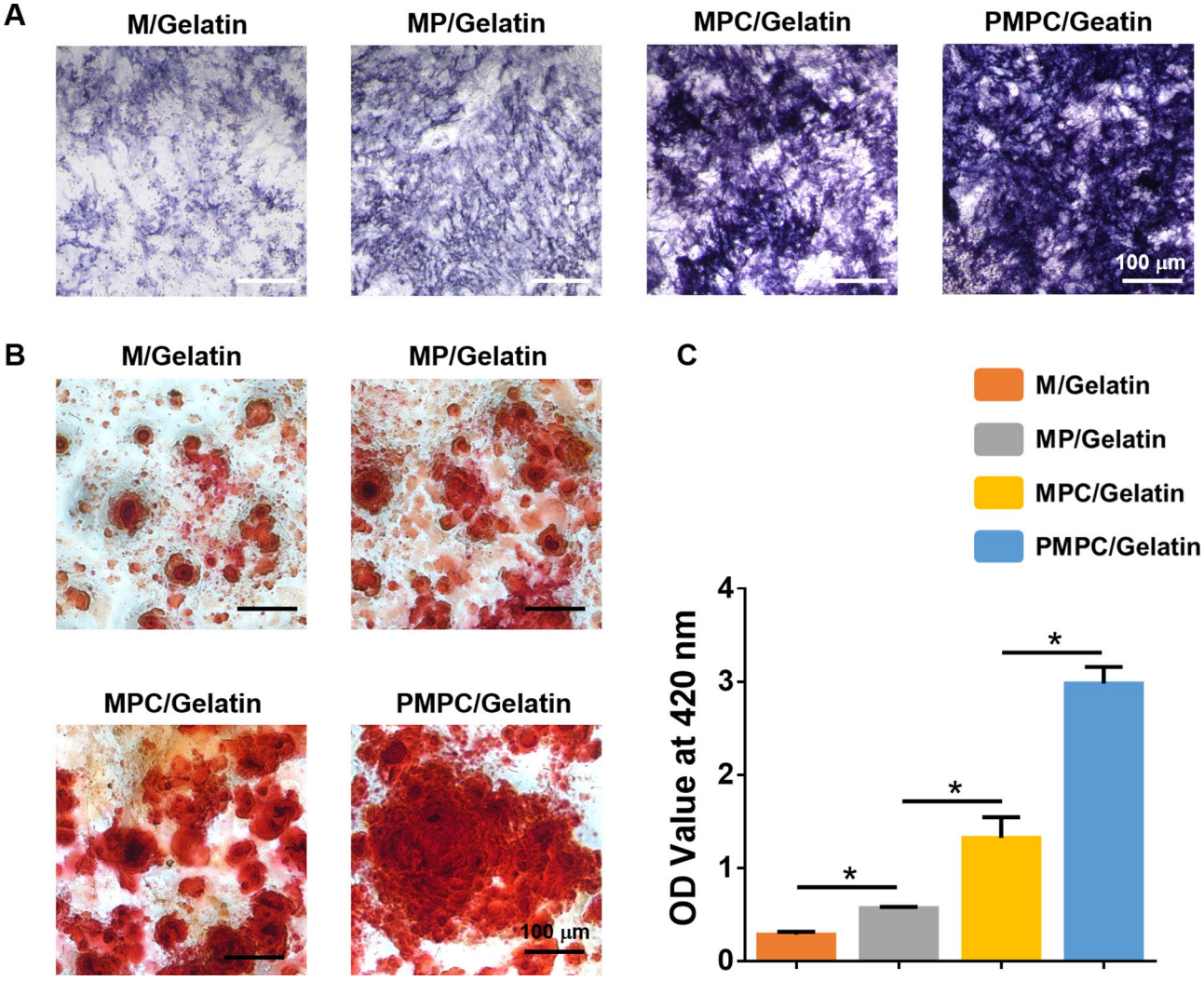

Fig. 5 In vitro osteogenesis of rBMSCs cultured with composite scaffolds. **(A)** ALP staining of the rBMSCs treatment with composite scaffolds after osteogenic induction for 7 days. **(B)** Alizarin red staining of the rBMSCs treatment with composite scaffolds after osteogenic induction for 14 days. **(C)** Quantitative analysis of alizarin red staining. ∗, $p < 0.05$

of the implanted area towards the center. New bone formation was barely observable in the defect group 4 weeks post-surgery. Less new bone tissue was observed at the peripheral part of the defects in M/Gelatin, MP/Gelatin, and MPC/Gelatin groups. In contrast, notable new bone formation was observed in the PMPC/Gelatin group. After 8 weeks, newly formed bone nearly covered the defects in the PMPC/Gelatin group than in the other experimental groups.

In order to get full evidence of composite materials on the osteogenic activities. Immunohistochemistry was employed to examine OCN and CD31 expressions in bone tissue. OCN expression was significantly increased in the experimental groups compared to the Defect group after 4 and 8 weeks, with the strongest signal intensity in PMPC/Gelatin groups (Fig. 10A and B). Moreover, CD31, a marker of newborn endothelial cells, is commonly used for neonatal micro-vessel counting to investigate the angiogenesis of implanted materials. Hence, CD31 immunohistochemical staining was conducted at 4 weeks after the operation. A small number of micro-vessels were identified within the bone defect of M/Gelatin and MP/Gelatin groups, while a vascular lumen with a larger diameter surrounded by CD31-positive endothelial cells was identified in the MPC/Gelatin and PMPC/Gelatin groups. PMPC/Gelatin group formed numerous neo-vessels surrounded by more endothelial cells that were positively stained with CD31 by the 8 weeks (Fig. 10C and D).

Discussion

Here, we demonstrated the suitability of an oriented gelatin scaffold combined with PTH loaded Cu-coated MnO_2 NPs regarding antibacterial efficiency and bone regeneration. The proposed therapeutic system's mechanisms

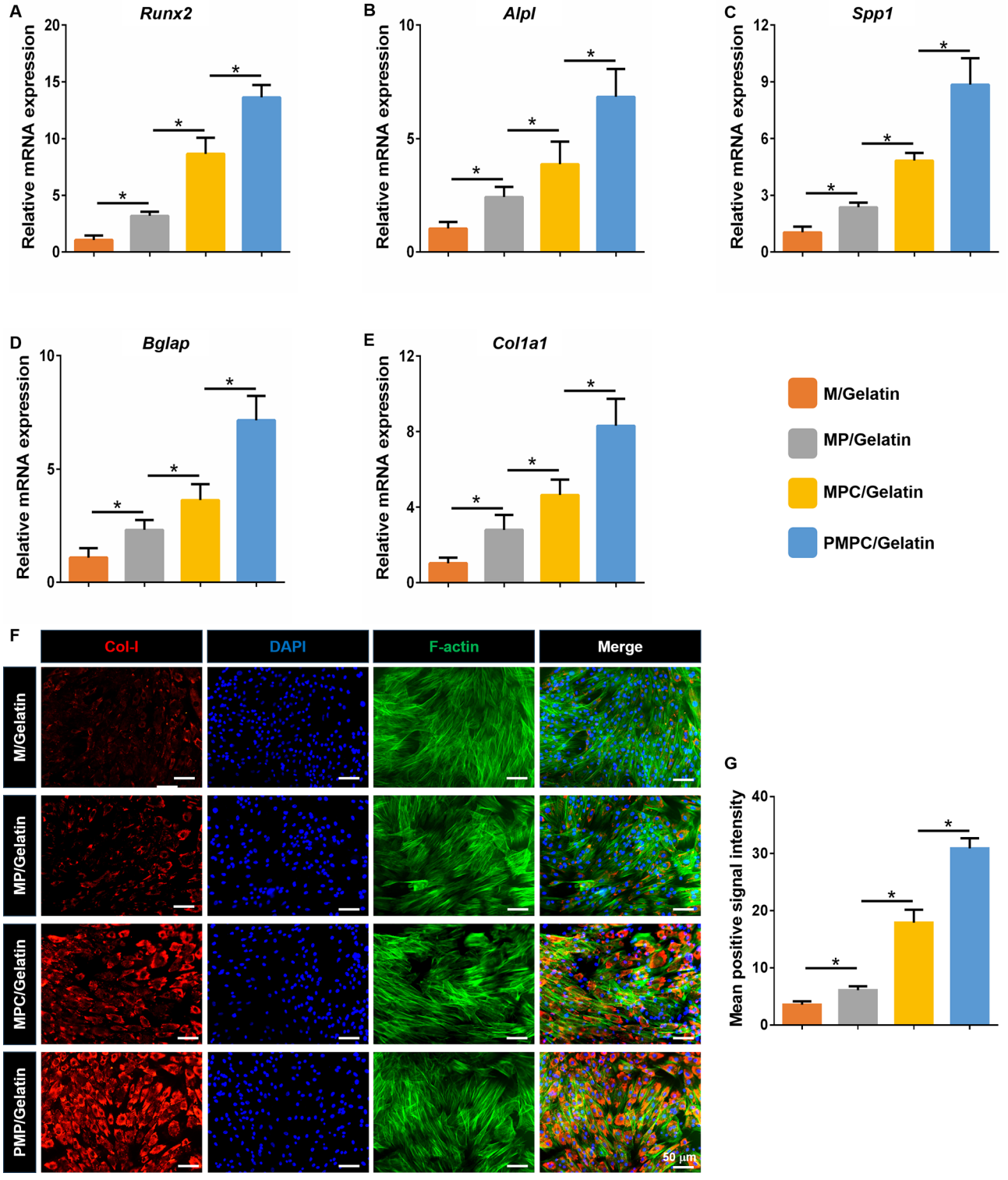

Fig. 6 Expression of osteogenesis-related genes and proteins in rBMSCs cultured with composite scaffolds. **(A-E)** Relative gene expression of *Runx2*, *Alpl*, *Spp1*, *Bglap*, and *Col1a1* of rBMSCs in the M/Gelatin, MP/Gelatin and MPC/Gelatin groups, respectively. *Gapdh* was used as the housekeeping gene. **(F)** The protein level of Col-I was detected by immunofluorescence in the M/Gelatin, MP/Gelatin and MPC/Gelatin group. **(G)** Quantification of the signal intensity of Col I. ∗, $p < 0.05$

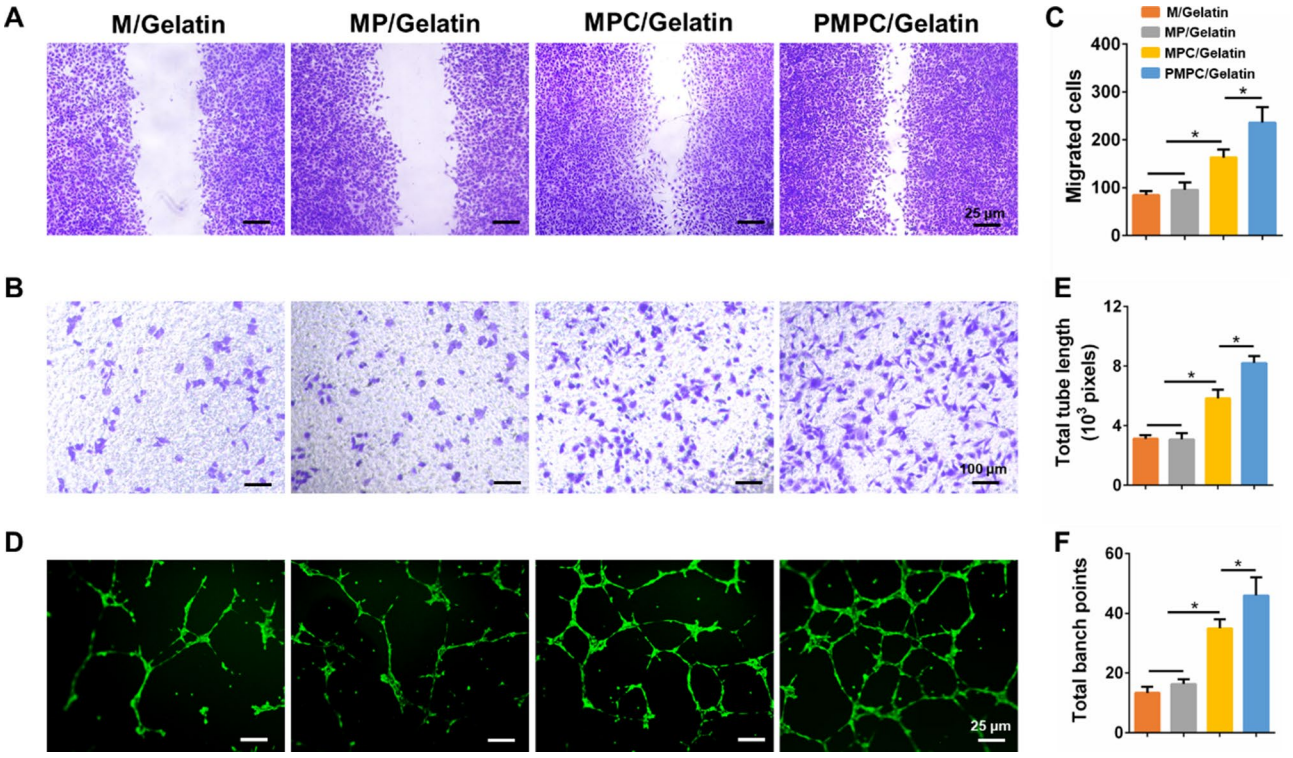

Fig. 7 Evaluation of the pro-angiogenic effect of composite scaffolds in vitro. **(A-B)** HUVEC migration among different groups was examined using wound healing and transwell assays, respectively. **(C)** Quantitation of migrated cells of transwell assay. **(D)** Representative images of the tube formation assay. **(E-F)** Quantitation of total tube length and total branch points, respectively. ∗, $p < 0.05$

and effectiveness were validated in vitro and in vivo using rBMSCs and an infected rat bone defect, respectively. Growing evidence suggests that bacterial metabolism and infection could induce a unique microenvironment with an acidity increase, which can be used to develop pH-responsive biomaterials to eradicate bacteria [40]. According to previous studies, bone defect creation triggers inflammation and blood vessel rupture, causing local acidosis [41]. Moreover, an infected microenvironment could decrease to moderately acidic (pH 5.5–6.7) or even lower as 3.5 [42]. A normal pH is necessary to maintain cellular functions, while an excessively acidic environment significantly inhibits osteoblast proliferation and collagen synthesis [43]. Besides, ROS overproduction is a critical factor in several pathological bone disorders, such as osteomyelitis [44]. Excessive ROS accumulation is closely related to cell senescence and apoptosis and could trigger bone destruction events due to the lower antioxidant enzyme levels and a block in osteoblast differentiation [45]. Therefore, targeting the infectious microenvironment to eliminate bacteria and improve cell survival environment is a promising approach for treating infected bone defect.

The attention-grabbing properties of MnO_2 NPs involve their decomposition in the presence of H^+ or glutathione [46]. Moreover, their nanostructures have the capability to induce H_2O_2 decomposition into oxygen and water [47]. These attributes augment the therapeutic potential of MnO_2 NPs as a biodegradable material responsive to the microenvironment. They can rise the pH level and decompose ROS that impair the osteogenesis process, presenting their potential as promising nanotherapeutics for scavenging free radicals and mitigating oxidative stress. In our study, we successfully synthesized MnO_2 NPs with hollow and spherical structures. Importantly, these NPs demonstrated negligible toxicity to rBMSCs, even at concentrations as high as 50 μg/mL. In vitro experiments demonstrated that MnO_2 NPs embed into gelatin scaffold could respond to pH change and protect cell from H_2O_2 damage, including cell senescence and death, decreased mitochondrial activity and increased ROS level. According to its performance in antimicrobial, M/Gelatin group displayed a slightly inhibited bacteria growth. Therefore, we used the reducing properties of dopamine to coat Cu on the surface of MnO_2 (MPC) NPs to increase antibacterial efficiency.

The Cu and Cu^{2+} are strong antimicrobial agents with a broad antibacterial spectrum [48, 49]. This metal is indispensable for all living organisms due to its involvement in various physiological functions, including angiogenesis, tissue formation, energy production, and multiple metabolic processes as enzyme cofactors [50]. Cu contributes

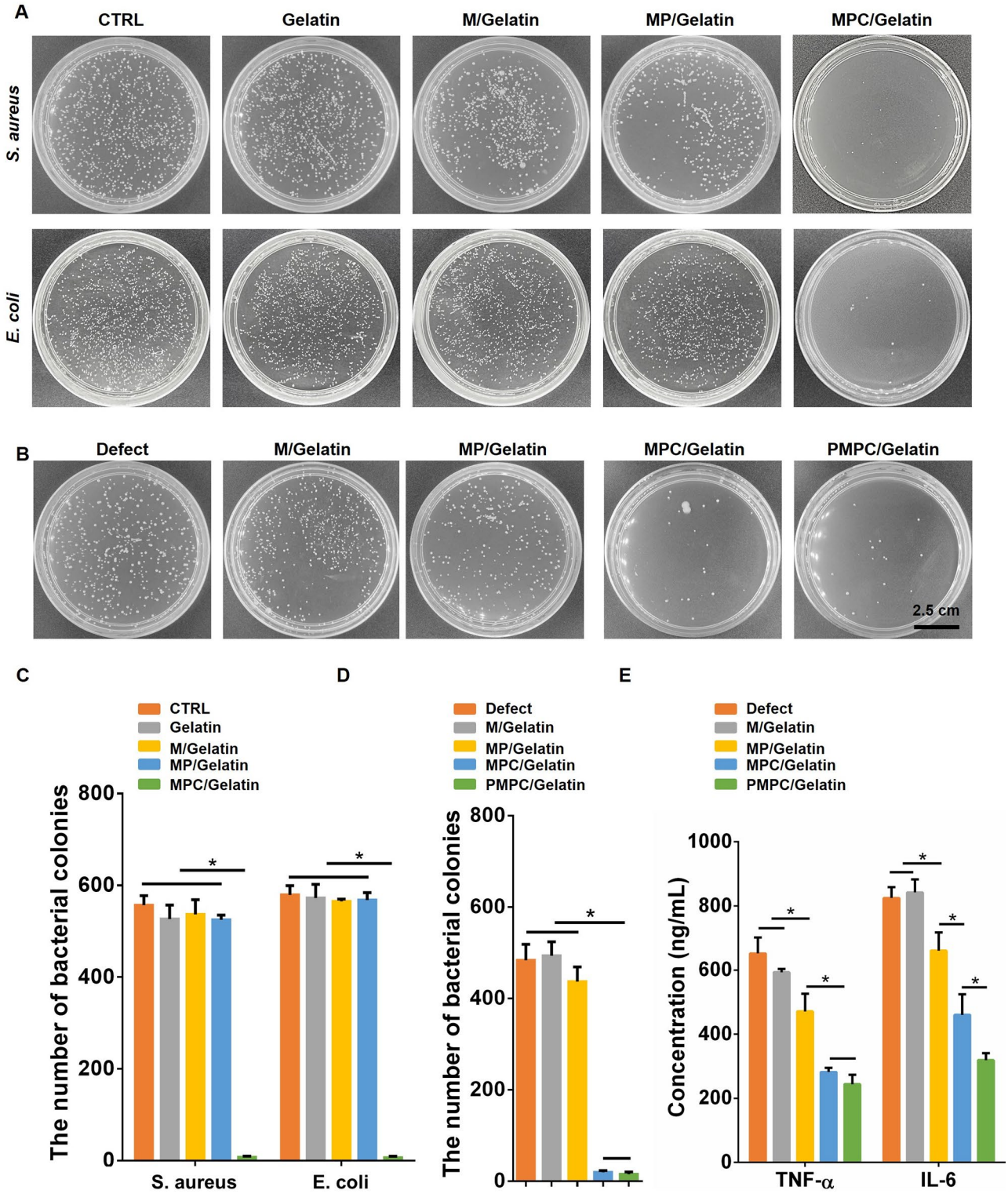

Fig. 8 Antibacterial measurement of composite scaffolds. Representative photographs of bacterial colonies of composite scaffolds in vitro **(A)** and in vivo **(B)**. Bacterial counts of different groups of in-vitro **(C)** and in-vivo **(D)** experiments. **(E)** Protein expression of TNF-α and IL-6 at 7 days after composite scaffold implantation. ∗, $p < 0.05$

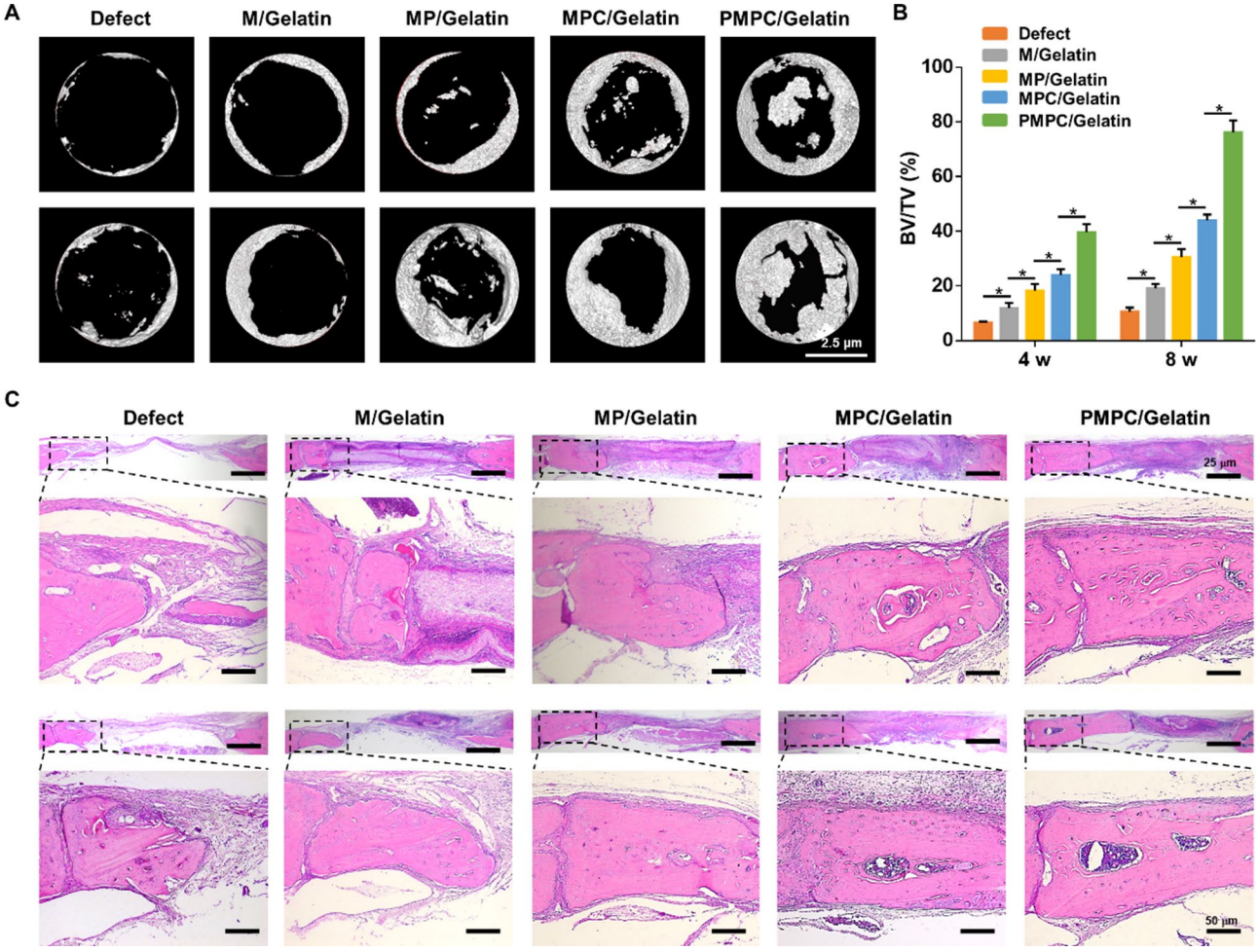

Fig. 9 Promotion of new bone formation by different materials at 4 and 8 weeks, respectively. **(A)** Micro-CT images with each group. **(B)** BV/TV values measured by micro-CT in different groups. **(C)** H&E staining of composite scaffolds in the repair of rat skull defects. *, $p < 0.05$

to maturation and growth of numerous tissue collagens, particularly in bone collagen [51]. It plays a vital role in osteoblast functions, bone mineralization, and vascularization [52]. Our data demonstrated that the composite scaffolds of gelatin combined with Cu-coated MnO_2 NPs (MPC/gelatin) had high antibacterial activity against *S. aureus*. In the presence of H_2O_2, cells treated with MPC/Gelatin had significantly higher levels of genes and proteins associated with osteogenesis than those treated with M/gelatin and MP/gelatin. Furthermore, PTH was encapsulated into MPC NPs to make the bone healing process steady and efficient. What's more, vasculogenic potential was obviously promoted of HUVECs in the MPC/Gelatin group. Interestingly, the synergistic effect of PTH and Cu was elucidated, presented as greatest angiogenesis found in the PMPC/Gelatin group. In this system, the gradual degradation of PMPC/Gelatin in infected bone defect site causes stable and sequential release of PTH and Cu, and then to function good positive effects on cells, enhancing vascularization, osteogenic differentiation and mineral deposition.

An infected skull defect model was established in rats by a trephine with 5 mm defects to further investigate the role of PMPC/Gelatin in vivo. After implantation for 14 days, our results revealed that MPC/Gelatin and PMPC/Gelatin groups had significant reductions in *S. aureus* survival and colony numbers compared to other groups, accompanied by a pronounced reduction in the production of pro-inflammatory factors, such as TNF-α and IL-6, two common indicators of ongoing infections. The release of Cu^{2+} had the potential to impede bacterial adherence and proliferation, thereby mitigating inflammatory responses. Additionally, at 4 and 8 weeks post-operation, the calvaria obtained from the Defect group displayed the development of thin and loose connective tissue, accompanied by a restricted amount of new bone formation within the infected defects. In contrast, the experimental groups exhibited enhanced new bone formation in the defects. Moreover, new bone formation

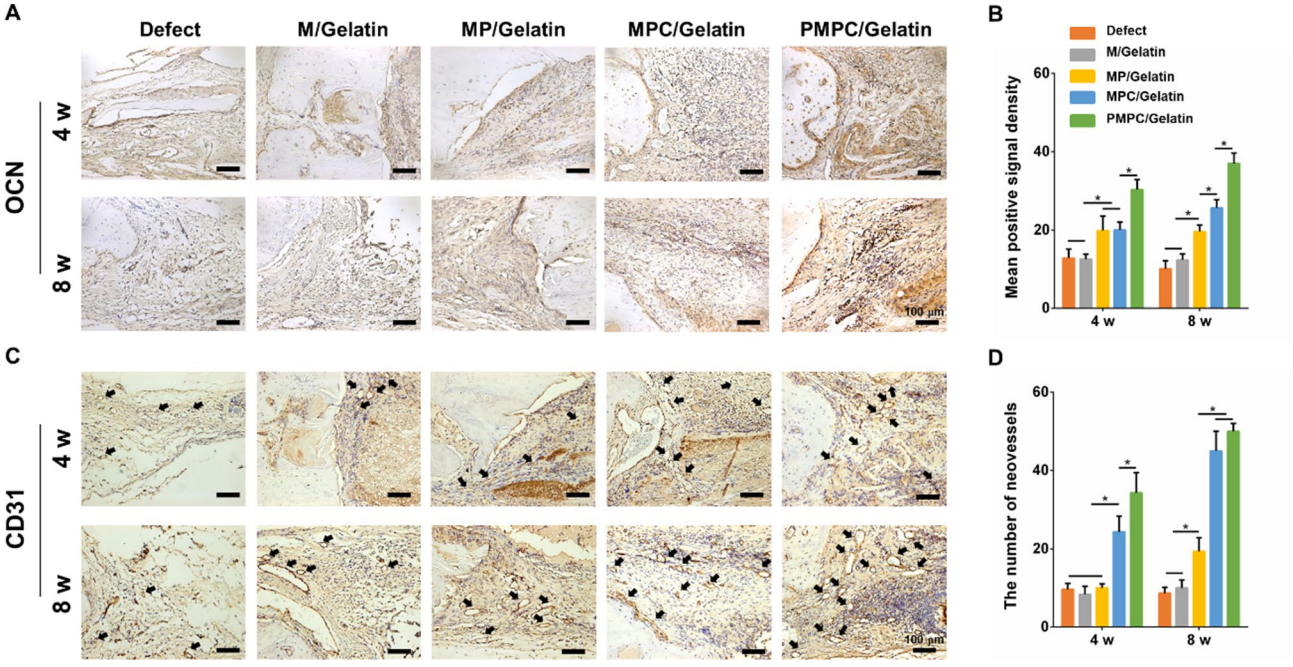

Fig. 10 Immunohistochemical analysis of OCN and CD31 expression in each group at 4 and 8 weeks, respectively. Representative images of the immunofluorescence of OCN **(A)** with semi-quantitative analysis **(B)**. **(C)** Representative images of the immunofluorescence of CD31. **(D)** Quantification of new vessels of different groups. *, $p < 0.05$

was even more impressive in the PMPC/Gelatin group compared with other experimental groups, which might be attributed to powerfully anabolic effect of PTH on bone cells. PMPC/Gelatin group consistently had a greater positive OCN immunohistochemistry intensity than other groups. We also performed CD31 staining to evaluate the neovascularization in the defects further. We observed numerous long and rounded vessels with different diameter in the MPC/Gelatin and PMPC/Gelatin groups, while minimal evidence of new vascularization was found in the M/Gelatin and Defect groups. These results proved the effects of copper on angiogenesis again. Further investigation is required to understand the effects of PMPC/Gelatin on immune cells, which are crucial for anti-infection responses and bone formation. Additionally, the functionality and efficacy of PMPC/Gelatin will be validated in large animal models.

Conclusion

This study introduced a new biomaterial exhibiting noteworthy antibacterial and osteo-inductive capabilities, demonstrated both in vitro and in vivo. The composite scaffold was adept at adapting to the bone infection microenvironment, actively contributing to pH reduction and ROS accumulation. Our investigation had successfully amalgamated the antibacterial attributes of copper (Cu) with the potent osteogenic properties of parathyroid hormone (PTH) within microenvironment-responsive MnO_2 NPs, integrated into an oriented gelatin scaffold. This innovative material showed promise for facilitating bone regeneration in the setting of contaminated bone defects. As a multifunctional scaffold, it holds potential as a therapeutic strategy for addressing infected bone defects like periapical bone lesions or contaminated bone fractures.

Acknowledgements

Not applicable.

Author contributions

Huilin Yang, Ling Liu, and Bin Li conceived and designed the study. Jiajia, Sun, Haidi Zhu, Huan Wang, and Jiaying Li performed the experiments and data analysis. Jiajia, Sun, Bin Li, Ling Liu, and Huilin Yang wrote the manuscript with input from all coauthors. All authors have read and approved the final version of the manuscript.

Funding

This work was support from the National Natural Science Foundation of China (Grant No. 81925027, 32271421), the Priority Academic Program Development of Jiangsu Higher Education Institutions, Science and Technology Development Plan Project of Suzhou (SYS2020095).

Data availability

No datasets were generated or analysed during the current study.

Declarations

Ethics approval and consent to participate

All procedures involving animals were approved by the Institutional Animal Care and Use Committee of Soochow University (SUDA20220711A09).

Consent for publication

All authors consent to the publication of the article.

Competing interests
The authors declare no competing interests.

Author details
[1]Medical 3D Printing Center, Orthopedic Institute, Department of Orthopedic Surgery, The First Affiliated Hospital, School of Biology and Basic Medical Sciences, Suzhou Medical College, Soochow University, Suzhou, Jiangsu 215000, China

Received: 5 February 2024 / Accepted: 31 August 2024
Published online: 19 September 2024

References

1. Caldwell M, Hughes M, Wei F, Ngo C, Pascua R, Pugazhendhi AS, Coathup MJ. Promising applications of D-amino acids in periprosthetic joint infection. Bone Res. 2023;11:14.
2. Manivasagam VK, Popat KC. Hydrothermally treated titanium surfaces for enhanced osteogenic differentiation of adipose derived stem cells. Mater Sci Eng C Mater Biol Appl. 2021;128:112315.
3. Shah NJ, Hyder MN, Moskowitz JS, Quadir MA, Morton SW, Seeherman HJ, Padera RF, Spector M, Hammond PT. Surface-mediated bone tissue morphogenesis from tunable nanolayered implant coatings. Sci Transl Med. 2013;5:191ra183.
4. Ghei A, Steijvers E, Xia Z. Manufacturing artificial bone allografts: a perspective. Biomater Transl. 2022;3:65–80.
5. Li D, Li Y, Shrestha A, Wang S, Wu Q, Li L, Guan C, Wang C, Fu T, Liu W, et al. Effects of programmed local delivery from a Micro/Nano-Hierarchical Surface on Titanium Implant on Infection Clearance and osteogenic induction in an infected bone defect. Adv Healthc Mater. 2019;8:e1900002.
6. Rasouli MR, Restrepo C, Maltenfort MG, Purtill JJ, Parvizi J. Risk factors for surgical site infection following total joint arthroplasty. J Bone Joint Surg Am. 2014;96:e158.
7. Wei P, Jing W, Yuan Z, Huang Y, Guan B, Zhang W, Zhang X, Mao J, Cai Q, Chen D, Yang X. Vancomycin- and strontium-loaded microspheres with multifunctional activities against Bacteria, in Angiogenesis, and in Osteogenesis for Enhancing infected bone regeneration. ACS Appl Mater Inter. 2019;11:30596–609.
8. Johnson EN, Burns TC, Hayda RA, Hospenthal DR, Murray CK. Infectious complications of open type III tibial fractures among combat casualties. Clin Infect Dis. 2007;45:409–15.
9. Jia WT, Fu Q, Huang WH, Zhang CQ, Rahaman MN. Comparison of Borate Bioactive Glass and Calcium Sulfate as implants for the local delivery of Teicoplanin in the treatment of Methicillin-Resistant Staphylococcus aureus-Induced Osteomyelitis in a rabbit model. Antimicrob Agents Ch. 2015;59:7571–80.
10. Inzana JA, Schwarz EM, Kates SL, Awad HA. Biomaterials approaches to treating implant-associated osteomyelitis. Biomaterials. 2016;81:58–71.
11. Hagberg K, Ghasemi Jahani SA, Omar O, Thomsen P. Osseointegrated prostheses for the rehabilitation of patients with transfemoral amputations: a prospective ten-year cohort study of patient-reported outcomes and complications. J Orthop Transl. 2023;38:56–64.
12. ter Boo GJ, Grijpma DW, Moriarty TF, Richards RG, Eglin D. Antimicrobial delivery systems for local infection prophylaxis in orthopedic- and trauma surgery. Biomaterials. 2015;52:113–25.
13. Yang H, Li Q, Wang X. Effect of radiation sterilisation on the structure and antibacterial properties of antimicrobial peptides. Biomater Transl. 2023;4:51–61.
14. Bai J, Feng Y, Li W, Cheng Z, Rosenholm JM, Yang H, Pan G, Zhang H, Geng D. Alternative copper-based single-atom Nanozyme with Superior Multienzyme activities and NIR-II responsiveness to fight against deep tissue infections. Res (Wash D C). 2023;6:0031.
15. Grass G, Rensing C, Solioz M. Metallic copper as an antimicrobial surface. Appl Environ Microbiol. 2011;77:1541–7.
16. Mitra D, Kang ET, Neoh KG. Antimicrobial copper-based materials and Coatings: potential multifaceted Biomedical Applications. Acs Appl Mater Inter. 2020;12:21159–82.
17. Guo Y, Chen C, Zhang S, Ren L, Zhao Y, Guo W. Mediation of mechanically adapted TiCu/TiCuN/CFR-PEEK implants in vascular regeneration to promote bone repair in vitro and in vivo. J Orthop Transl. 2022;33:107–19.
18. Dahl SL, Rucker RB, Niklason LE. Effects of copper and cross-linking on the extracellular matrix of tissue-engineered arteries. Cell Transpl. 2005;14:367–74.
19. Rodriguez JP, Rios S, Gonzalez M. Modulation of the proliferation and differentiation of human mesenchymal stem cells by copper. J Cell Biochem. 2002;85:92–100.
20. Rath SN, Brandl A, Hiller D, Hoppe A, Gbureck U, Horch RE, Boccaccini AR, Kneser U. Bioactive copper-doped glass scaffolds can stimulate endothelial cells in co-culture in combination with mesenchymal stem cells. PLoS ONE. 2014;9:e113319.
21. Chen Z, Zhao M, Zhang J, Zhou K, Ren X, Mei X. Construction of injectable, pH sensitive, antibacterial, mineralized amino acid yolk-shell microspheres for potential minimally invasive treatment of bone infection. Int J Nanomed. 2018;13:3493–506.
22. Cicuendez M, Doadrio JC, Hernandez A, Portoles MT, Izquierdo-Barba I, Vallet-Regi M. Multifunctional pH sensitive 3D scaffolds for treatment and prevention of bone infection. Acta Biomater. 2018;65:450–61.
23. Weinrick B, Dunman PM, McAleese F, Murphy E, Projan SJ, Fang Y, Novick RP. Effect of mild acid on gene expression in Staphylococcus aureus. J Bacteriol. 2004;186:8407–23.
24. Lew DP, Waldvogel FA. Osteomyelitis. Lancet. 2004;364:369–79.
25. Massaccesi L, Galliera E, Pellegrini A, Banfi G, Corsi Romanelli MM. Osteomyelitis, oxidative stress and related biomarkers. Antioxid (Basel) 2022, 11.
26. Chang CH, Qiu J, O'Sullivan D, Buck MD, Noguchi T, Curtis JD, Chen Q, Gindin M, Gubin MM, van der Windt GJ, et al. Metabolic competition in the Tumor Microenvironment is a driver of Cancer Progression. Cell. 2015;162:1229–41.
27. Ansari MY, Ahmad N, Haqqi TM. Oxidative stress and inflammation in osteoarthritis pathogenesis: role of polyphenols. Biomed Pharmacother. 2020;129:110452.
28. Yang G, Xu L, Chao Y, Xu J, Sun X, Wu Y, Peng R, Liu Z. Hollow MnO2 as a tumor-microenvironment-responsive biodegradable nano-platform for combination therapy favoring antitumor immune responses. Nat Commun. 2017;8:902.
29. Kumar S, Adjei IM, Brown SB, Liseth O, Sharma B. Manganese dioxide nanoparticles protect cartilage from inflammation-induced oxidative stress. Biomaterials. 2019;224:119467.
30. Li J, Han F, Ma J, Wang H, Pan J, Yang G, Zhao H, Zhao J, Liu J, Liu Z, Li B. Targeting endogenous hydrogen peroxide at bone defects promotes bone repair. Adv Funct Mater. 2022;32:2111208.
31. Wu N, Gao H, Wang X, Pei X. Surface modification of Titanium implants by Metal Ions and nanoparticles for Biomedical Application. ACS Biomater Sci Eng. 2023;9:2970–90.
32. Jin A, Wang Y, Lin K, Jiang L. Nanoparticles modified by polydopamine: Working as drug carriers. Bioact Mater. 2020;5:522–41.
33. Harrington MJ, Masic A, Holten-Andersen N, Waite JH, Fratzl P. Iron-clad fibers: a metal-based biological strategy for hard flexible coatings. Science. 2010;328:216–20.
34. Meng Y, Liu P, Zhou W, Ding J, Liu J. Bioorthogonal DNA adsorption on polydopamine nanoparticles mediated by metal coordination for highly robust sensing in serum and living cells. ACS Nano. 2018;12:9070–80.
35. Gensure RC, Gardella TJ, Juppner H. Parathyroid hormone and parathyroid hormone-related peptide, and their receptors. Biochem Biophys Res Commun. 2005;328:666–78.
36. Wein MN, Kronenberg HM. Regulation of bone remodeling by parathyroid hormone. Cold Spring Harb Perspect Med 2018, 8.
37. Wojda SJ, Donahue SW. Parathyroid hormone for bone regeneration. J Orthop Res. 2018;36:2586–94.
38. Baranowsky A, Jahn D, Jiang S, Yorgan T, Ludewig P, Appelt J, Albrecht KK, Otto E, Knapstein P, Donat A, et al. Procalcitonin is expressed in osteoblasts and limits bone resorption through inhibition of macrophage migration during intermittent PTH treatment. Bone Res. 2022;10:9.
39. Paridis D, Karachalios T. Atrophic femoral bone nonunion treated with 1–84 PTH. J Musculoskelet Neuronal Interact. 2011;11:320–2. quiz 323.
40. Liu B, Li J, Zhang Z, Roland JD, Lee BP. pH responsive antibacterial hydrogel utilizing catechol-boronate Complexation Chemistry. Chem Eng J 2022, 441.
41. Walters G, Pountos I, Giannoudis PV. The cytokines and micro-environment of fracture haematoma: current evidence. J Tissue Eng Regen Med. 2018;12:e1662–77.
42. Machado A, Pereira I, Silva V, Pires I, Prada J, Poeta P, Costa L, Pereira JE, Gama M. Injectable hydrogel as a carrier of Vancomycin and a cathelicidin-derived peptide for osteomyelitis treatment. J Biomed Mater Res A. 2022;110:1786–800.

43. Arnett TR. Extracellular pH regulates bone cell function. J Nutr. 2008;138:S415–8.
44. Grbic R, Miric DJ, Kisic B, Popovic L, Nestorovic V, Vasic A. Sequential analysis of oxidative stress markers and vitamin C status in acute bacterial osteomyelitis. Mediat Inflamm. 2014;2014:975061.
45. Chen W, Zhang H, Zhou Q, Zhou F, Zhang Q, Su J. Smart Hydrogels for Bone Reconstruction via modulating the Microenvironment. Res (Wash D C). 2023;6:0089.
46. Fan W, Bu W, Shen B, He Q, Cui Z, Liu Y, Zheng X, Zhao K, Shi J. Intelligent MnO2 Nanosheets anchored with Upconversion Nanoprobes for Concurrent pH-/H2O2-Responsive UCL imaging and oxygen-elevated synergetic therapy. Adv Mater. 2015;27:4155–61.
47. Gordijo CR, Abbasi AZ, Amini MA, Lip HY, Maeda A, Cai P, O'Brien PJ, Dacosta RS, Rauth AM, Wu XY. Hybrid Nanoparticles: Design of Hybrid MnO2-Polymer-Lipid Nanoparticles with Tunable Oxygen Generation Rates and Tumor Accumulation for Cancer Treatment (Adv. Funct. Mater. 12/2015). *Adv Funct Mater* 2015.
48. Zhuang Y, Zhang S, Yang K, Ren L, Dai K. Antibacterial activity of copper-bearing 316L stainless steel for the prevention of implant-related infection. J Biomed Mater Res B Appl Biomater. 2020;108:484–95.
49. Vimbela GV, Ngo SM, Fraze C, Yang L, Stout DA. Antibacterial properties and toxicity from metallic nanomaterials. Int J Nanomed. 2017;12:3941–65.
50. Chellan P, Sadler PJ. The elements of life and medicines. Philos Trans Math Phys Eng Sci 2015, 373.
51. Opsahl W, Zeronian H, Ellison M, Lewis D, Rucker RB, Riggins RS. Role of copper in collagen cross-linking and its influence on selected mechanical properties of chick bone and tendon. J Nutr. 1982;112:708–16.
52. Lowe NM, Lowe NM, Fraser WD, Jackson MJ. Is there a potential therapeutic value of copper and zinc for osteoporosis? Proc Nutr Soc. 2002;61:181–5.

Publisher's note